Applied Catalysis B: Environmental 310 (2022) 121297

Contents lists available at ScienceDirect

Applied Catalysis B: Environmental

journal homepage: www.elsevier.com/locate/apcatb

# Bamboo-inspired design of a stable and high-efficiency catalytic capillary microreactor for nitroaromatics reduction

Jingpeng Li [a,b], Rumin Ma [a], Yun Lu [c,*], Zaixing Wu [a], Rong Liu [b], Minglei Su [b], Xiaobei Jin [b], Rong Zhang [b], Yongjie Bao [a], Yuhe Chen [a], Daochun Qin [b,*], Dongjiang Yang [d,*], Zehui Jiang [b,*]

[a] Key Laboratory of High Efficient Processing of Bamboo of Zhejiang Province, Engineering Technology Research Center for Building and Decorating Materials of Bamboo State Forestry Administration, China National Bamboo Research Center, Hangzhou 310012, China
[b] Key Laboratory of Bamboo and Rattan Science & Technology, International Center for Bamboo and Rattan, Beijing 100102, China
[c] Research Institute of Wood Industry, Chinese Academy of Forestry, Beijing 100091, China
[d] State Key Laboratory of Bio-fibers and Eco-textiles, Collaborative Innovation Center of Shandong Marine Biobased Fibers and Ecological textiles, Institute of Marine Biobased Materials, School of Environmental Science and Engineering, Collage of Materials Science and Engineering, Qingdao University, Qingdao 266071, China

ARTICLE INFO

*Keywords:*
Bamboo-inspired design
High efficiency
Capillary microreactor
Ag catalyst
Nitroaromatics

ABSTRACT

A stable and high-efficiency bamboo-inspired catalytic capillary microreactor (CMR) decorated with Ag nanoparticles (NPs) is skillfully designed for the continuous-flow reduction of nitroaromatics. By a novel continuous-flow method, Ag NPs are mainly dispersed around the long microchannels uniformly and firmly in bamboo vascular bundle. The bioinspired CMR achieves a continuously effective fluid flow while maintaining the high reactivity of Ag catalyst in the reduction of four nitroaromatics and shows good long-term stability where the catalytic performance remained at 90% within 11 h of five cycles. The detection of $H^{\bullet}$ radical adducts indicated that Ag NPs adsorb the $BH_4^-$ ions to form the Ag–H species. The exceptional pore channel of CMR with a large surface area provides active sites readily accessible and facilitates $H^{\bullet}$ radicals and electrons transfer to sinaficantly enhance nitroaromatic reduction. This sustainable bamboo-inspired design can greatly impel the future development of renewable catalysis system for wider applications.

## 1. Introduction

Heterogeneous catalytic reactions are widely used in the chemical and pharmaceutical industries. Over the past two decades, the microreactor technologies have shown great potential in heterogeneous catalytic reactions including Heck, Sonogashira, Suzuki, Kumada, olefin metathesis, hydrogenation, and benzannulation reactions [1,2]. The high surface area-to-volume ratio in microreactors promotes high mass and heat transfer rates. Microreactors also often provide efficient mixing, high conversion, and selectivity. In addition, they minimize the reagent and solvent requirements, thus reducing the environmental and safety issues associated with catalysis [3]. For gram-scale synthesis, a number of microreactors should be used in parallel [4]. Meanwhile, various materials and techniques have been widely developed to construct microreactors. Early microreactors were microfabricated on chips or plates using substrates like silicon and glass [5]. Nowadays, with the rapid expansion of flow chemistry, affordable and readily available capillary microreactors (often based on polymer, ceramics, and stainless steel) have become popular. However, the current strategies for the preparation of microreactors with narrow inner diameter channels of less than 1 mm typically involve troublesome procedures, toxic chemicals, high energy consumption, and unrenewable resources. These issues lead to increased production cost and environmental pollution [1,2,5].

Nature is an important source of inspiration for scientists. Advanced technologies have been developed from the understanding of the complex relationship between structure and function of matter [6,7]. There has been increasing interest in the development of more effective and simple microchannel devices, which are composed of inexpensive and naturally abundant materials. For example, the fabrication of natural material-based devices including a 3D Pd/wood membrane [8], Ag/wood filter [9], 3D Ag/rattan filter [10], 3D Au/sugarcane membrane [11], Ag/sugarcane filter [12], bamboo-based analytical device [13], bamboo-based microreactor [14], “bambootronic” device [15], and bamboo-based solar steam device [16] have recently been reported. Particularly, 3D membrane/filter-based catalytic microreactors have

* Corresponding authors.
*E-mail addresses:* y.lu@caf.ac.cn (Y. Lu), qindc@icbr.ac.cn (D. Qin), d.yang@qdu.edu.cn (D. Yang), jiangzehui@icbr.ac.cn (Z. Jiang).

https://doi.org/10.1016/j.apcatb.2022.121297
Received 18 December 2021; Received in revised form 4 March 2022; Accepted 5 March 2022
Available online 8 March 2022

been typically synthesized by a static method. Previous studies have found that the preparation of bamboo-based devices is more suitable by the flow method [13–15]. To improve catalytic efficiency and reduce costs, catalytic reactions in continuous-flow systems have been recommended. The activity of catalysts in microchannels is preserved even when the reactants are flowed through the channels. Therefore, a continuous-flow strategy that uses uniform catalysts layers on the inner surface of a microreactor with a very large specific interfacial area per unit of volume (10,000–50,000 $m^2/m^3$) is preferred over a static system [3,17]. Bamboo, a naturally abundant material, is one of the best candidates for fabricating the CMR. The long microchannels in its vascular tissue have a high surface area-to-volume ratio of above 31,000 $m^2/m^3$ (see supporting information) [18]. Bamboo also grows rapidly and can be harvested every 3–5 years, which is better than the 20–60 years growth cycle of traditional timber [19]. Moreover, bamboo is cheap (0.07 USD/Kg) [20] especially when compared with traditional catalyst supports [21].

Through evolution over hundreds of millions of years, bamboo possesses a rational and superior microstructure and function that allowed them to flourish in land. A living bamboo constantly transports water and inorganic salts from the ground to upstream using xylem microchannels via the natural transpiration process. Meanwhile, its phloem microchannels transport nutrients over long distances via capillary action [22]. Previous studies have found that the metal NPs with different surface charges can also be transported through a plant's vascular system including the xylem and phloem [23,24]. These processes might find many applications in electrocatalyst, water desalination, microfluidic analytical device, biodetection, and bioseparation [14,25,26].

Herein, inspired by the transpiration process and superior microstructure and function of bamboo, we propose a "bamboo-inspired design" using natural bamboo as a biotemplate for catalysis. Bamboo was decorated with Ag NPs within its microchannels for stable and high-efficiency CMR. The bamboo-inspired microreactor possesses several interesting characteristics, which are discussed below. (1) The bamboo was used as a reductant and support for an in situ synthesis of uniformly distributed and stable Ag NPs. (2) The Ag NPs were mainly concentrated around the microchannels of vascular bundle, which optimized the use of the catalysts. The preparation was facile, cost effective, and easy to scale-up. (3) An efficient continues-flow use of catalysts without a tedious catalyst recycle process. This could avoid the waste of catalyst. (4) An effective interaction between reactants, substrates, and Ag catalyst due to the extremely large interfacial areas and short path required for nitroaromatic diffusion in the bamboo microchannel space. (5) The bamboo-inspired microreactor was stable and reusable for the catalytic conversion of nitroaromatics with $NaBH_4$. (6) Finally, the excellent mechanical property of the microreactor enabled its use in long-term flow catalytic applications.

## 2. Materials and methods

### 2.1. Materials

Moso bamboo (*Phyllostachys edulis*), which is widely distributed in South China, was used to fabricate the flow microreactors. The bamboo was obtained from Fujian, China. The bamboo sticks with dimensions of $\Phi$10 mm × 200 mm (growth direction) were obtained from the bamboo internodes. The internode culms from 1.2 to 1.8 m aboveground with a wall thickness ranging from 1.2 to 1.4 cm were selected for this study. Silver nitrate ($AgNO_3$), ammonium hydroxide ($NH_4OH$, 26–28%), sodium borohydride ($NaBH_4$), 4-nitrophenol (4-NP), 2-nitrophenol (2-NP), 4-nitroaniline (4-NA), and 2-nitroaniline (2-NA) were purchased from Aladdin Chemistry Co., Ltd (Shanghai, China) and used without modifications. Purified water was obtained from a Milli-Q® Advantage A10 water purification system from Millipore (MA, USA).

### 2.2. Fabrication of bamboo-inspired CMR

The Ag NPs were anchored onto the walls of bamboo microchannels by mimicking the water transport process relying on the microchannels via transpiration of bamboo. The bamboo sticks with straight microchannels were directly used to reduce $Ag(NH_3)_2^-$ ions and anchor the formed Ag NPs. First, fresh $Ag(NH_3)_2NO_3$ solution was prepared by dropwise addition of 10% aqueous ammonia into 30 mL $AgNO_3$ aqueous solution until the brown precipitates dissolved and a clear solution was produced. The fresh $Ag(NH_3)_2NO_3$ solution was then pumped to circularly flow through the bamboo sticks using a peristaltic pump at a flow rate of 0.3 mL/min. Note that the bamboo sticks were wrapped around with 3 M tape to avoid the leaching of liquid. Both ends of bamboo sticks were closely connected with silicone tube to construct continuous-flow preparation system. During this process, the $Ag(NH_3)_2^+$ ions were gradually reduced to form Ag NPs. After 12 h, the bamboo was washed with purified water until the pH of the washing solution reached 7. The washed bamboo was then dried at 45 °C for 24 h to obtain the bamboo-inspired CMR. The bamboo samples with varying $AgNO_3$ concentrations of 8, 20, and 50 mM were denoted as Ag-1/B CMR, Ag-2/B CMR, and Ag-3/B CMR, respectively.

For comparison, a bamboo stick sample that was entirely immersed in 50 mM $Ag(NH_3)_2NO_3$ was reacted for 24 h under vacuum. Other reaction conditions were the same as in the flow method above.

### 2.3. Characterization

The surface morphology is characterized by a field emission scanning electron microscope (SEM, Hitachi SU8010, Tokyo, Japan) and an Olympus SZ61 stereomicroscope (Olympus, Tokyo, Japan). The elemental distribution was examined by energy dispersive X-ray spectroscopy (EDS, Bruker Xflash 6130). The porosity of the sample was obtained via mercury intrusion method using a MicroActive AutoPore V 9600 (Micromeritics, America). X-ray diffraction (XRD) patterns of the block samples were collected using a Rigaku Ultima IV X-ray diffractometer with Cu Kα radiation. XPS measurements were acquired using a Thermo ESCALAB 250Xi spectrometer (Thermo Scientific, Waltham, MA, USA) with an Al K X-ray source. The transmission electron microscopy (TEM) images were performed on a field-emission transmission electron microscope (FE-TEM, FEI Talos F200S, USA). The samples were scraped from the Ag-loaded microchannels in vascular bundle under a microscope and supported on a Cu grid for TEM analysis. The existence of Ag in the microchannel was analyzed using the time-of-flight secondary ion mass spectroscopy (ToF-SIMS; PHI nanoTOF II, USA). The mechanical property was determined using a universal material testing machine (CMT 6103, Sans Testing Machine Inc., Shenzhen, China). The detection of $H^•$ radical species was conducted in a batch fashion. Electron paramagnetic resonance (EPR) spectra were recorded with Bruker EMX PLUS spectrometer (Germany) with a resonance frequency of 9.82 GHz with power of 6.325 mW. To quantify the Ag loading in bamboo, the absolute dried Ag/bamboo was cut to pieces and completely dissolved in to aqua regia to be tested by inductively coupled plasma mass spectrometry (ICP-MS, Agilent 7700). Zeta potential was measured based on Chinese national standards GB/T 37617–2019 using a SurPASS Electrokinetic Analyzer equipped with an adjustable gap cell from Anton Paar GmbH (Graz, Austria). Bamboo sample was processed into slices with a size of 10 mm × 20 mm and a thickness of ~1 mm. Test conditions: Electrolyte solution temperature: 25 ± 2 °C; Electrolyte solution concentration: 1 mmol/L KCl; Best pH range: 3–10; Test pressure: 0.03 MPa; Flow rate: (100 ± 20) mL/min. The pH was adjusted by using 0.1 mol/L hydrochloric acid or 0.1 mol/L sodium hydroxide solution.

### 2.4. Catalytic performance of the bamboo-inspired CMRs

The reduction of nitroaromatics (4-NP, 2-NP, 4-NA, and 2-NA) were used to evaluate the catalytic performance of the prepared bamboo-

inspired CMRs. Here 0.5 mM of a nitroaromatic and freshly prepared 0.25 M $NaBH_4$ were mixed and immediately flowed through the microreactor at a certain flow rate. The products were collected from the microreactor outlet and analyzed by UV/Vis spectroscopy at 400, 415, 380, and 412 nm for 4-NP, 2-NP, 4-NA, and 2-NA, respectively using a UV-2550 from Shimadzu (Kyoto, Japan) [27]. The conversion efficiency (%) of nitroaromatics were calculated using the equation: conversion efficiency (%) = $100 \times (A_0 - A)/A_0$ where $A_0$ and A were the concentration of a nitroaromatic in the sample influent and effluent solution, respectively.

The leaching of Ag NPs in the flow CMR was also investigated using the Ag-3/B CMR [28]. Briefly, 10 mL of the purified water was circularly flowed through the microreactor for 12 h with a flow speed of 120 μL/min. The concentration of Ag ions in the washing solution is 181.6 ppb by ICP-MS. After this washing for 12 h, 1 mL aliquot of the washing solution was mixed with 2 mL of a mixed aqueous solution that contained 0.5 mM 4-NP and 0.25 mM $NaBH_4$. The resulting solution was stored at room temperature for 5 days. If the yellow color of the solution gradually faded during storage, this indicated the serious leaching of Ag NPs from the sample.

## 3. Result and discussion

The prepared capillary microreactor for continuous-flow catalysis is derived from the natural bamboo, which was able to pump water up to over a record 45 m in height (Fig. 1a). To mimic the water pumping process in the prepared capillary microreactor, a bamboo stick sample was obtained by cutting perpendicular to the growth direction of living bamboo. The bamboo components of lignin, cellulose, and hemicellulose participated in the reduction process of $[Ag(NH_3)_2]^+$ ions to produce Ag NPs [10]. The Ag NPs were then deposited on the walls of the long and interconnected microchannels inside the vascular bundles of bamboo to form the CMR (Fig. 1b). Our continuous-flow method avoided the use of additional reductants and energy-consuming steps such as vacuum [9], carbonization [29], and hydrothermal treatment [30]. It also reduced the amount of noble metal catalysts, thus effectively lowering the cost of the reactors [31]. After uniform Ag NPs decoration by the in situ approach, all the structural characteristics in natural bamboo were well preserved in the capillary microreactor. Since the layer of Ag NPs was very thin, no obvious blockage was observed and ensured the continuous transport of liquid inside the microchannels. As a result, the Ag NPs decorated bamboo microreactor demonstrated excellent catalytic activity and stability. This was attributed to its flow-through and regular microchannel structures with a low tortuosity for transporting nitroaromatic molecules (Fig. 1c). We achieved interaction between reactants, substrate, and an Ag catalyst using the extremely large interfacial areas and short path required for molecular diffusion in the very narrow channel space.

### 3.1. Fabrication and characterization of the bamboo-inspired CMR

Bamboo can be easily processed into sticks with various sizes using a bamboo wire drawing machine. The bamboo sticks possessed a uniform column shape with a diameter ~10 mm as shown in Fig. 2b. Bamboo has a heterogeneous structure. The numerous vascular bundles, which were embedded within a matrix of ground parenchyma cells were observed in the transection (Fig. 2b, inset). The vascular bundle system consisted of the two metaxylem vessels, fibers, and metaphloem of sieve tubes with companion cells as observed by SEM (Fig. 2c). The lined-up straight microchannels (Fig. 2d) in the vascular bundle system were very important for the fluid transport. According to our previous work, Ag NPs can be synthesized in situ on the internal microchannels of rattan by impregnating the rattan cane with $Ag(NH_3)_2NO_3$ solution under vacuum [10]. However, we were not able to prepare the Ag NPs using same method, although the diameter of the bamboo sample (10 mm) was less than rattan (37.5 mm) (Fig. S1). In addition, the reaction only worked when the sample solution was flowed through a catalytic reactor. Thus, a facile continuous-flow method was applied to realize the synthesis and immobilization of Ag NPs on the walls of microchannels. We observed good dispersion even though the bamboo sample was 200 mm long (Fig. S2). This strategy optimized the use of silver in the reaction during the flow process.

Numerous pits adorned the inner surface of the long protoxylem vessel channel in vascular bundle system as shown in Fig. 2d and Fig. S3 (magnified SEM image of Fig. 2d). The hierarchical pore structure in the bamboo sample created a high surface area, which was suitable for the efficient preparation of Ag NPs. It also allowed the bamboo sample to be applied in a flow system. The bamboo sample was successfully applied to reduce the $Ag^+$ without adding any reductants or stabilizers as shown in Fig. 2e–g. The amount of Ag NPs produced was increased with the increase of the $Ag(NH_3)_2NO_3$ concentration. The Ag NPs with good dispersion was mainly formed in the microchannel array. This was

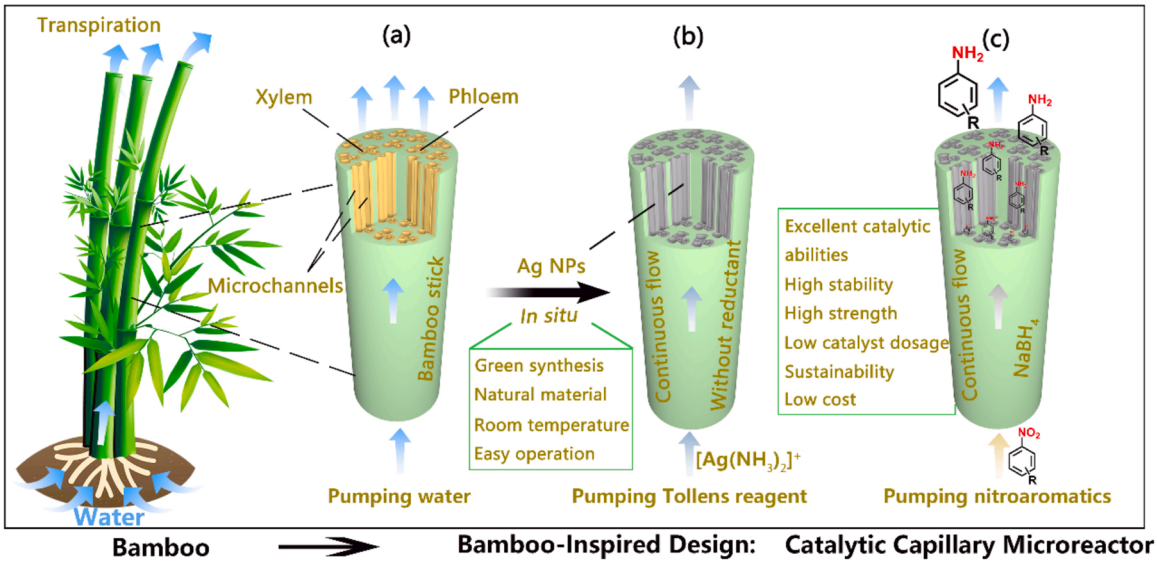


**Fig. 1.** Bamboo-inspired CMR design. (a) Schematic of a living bamboo that is continuously transporting water from the ground to upstream through the bamboo microchannels via the transpiration process. (b) The continuous-flow synthesis of Ag NPs on the walls of microchannels of bamboo without adding any external reductant. (c) The Ag NPs decorated bamboo stick can function effectively as a stable continuous-flow CMR due to its well aligned channels.

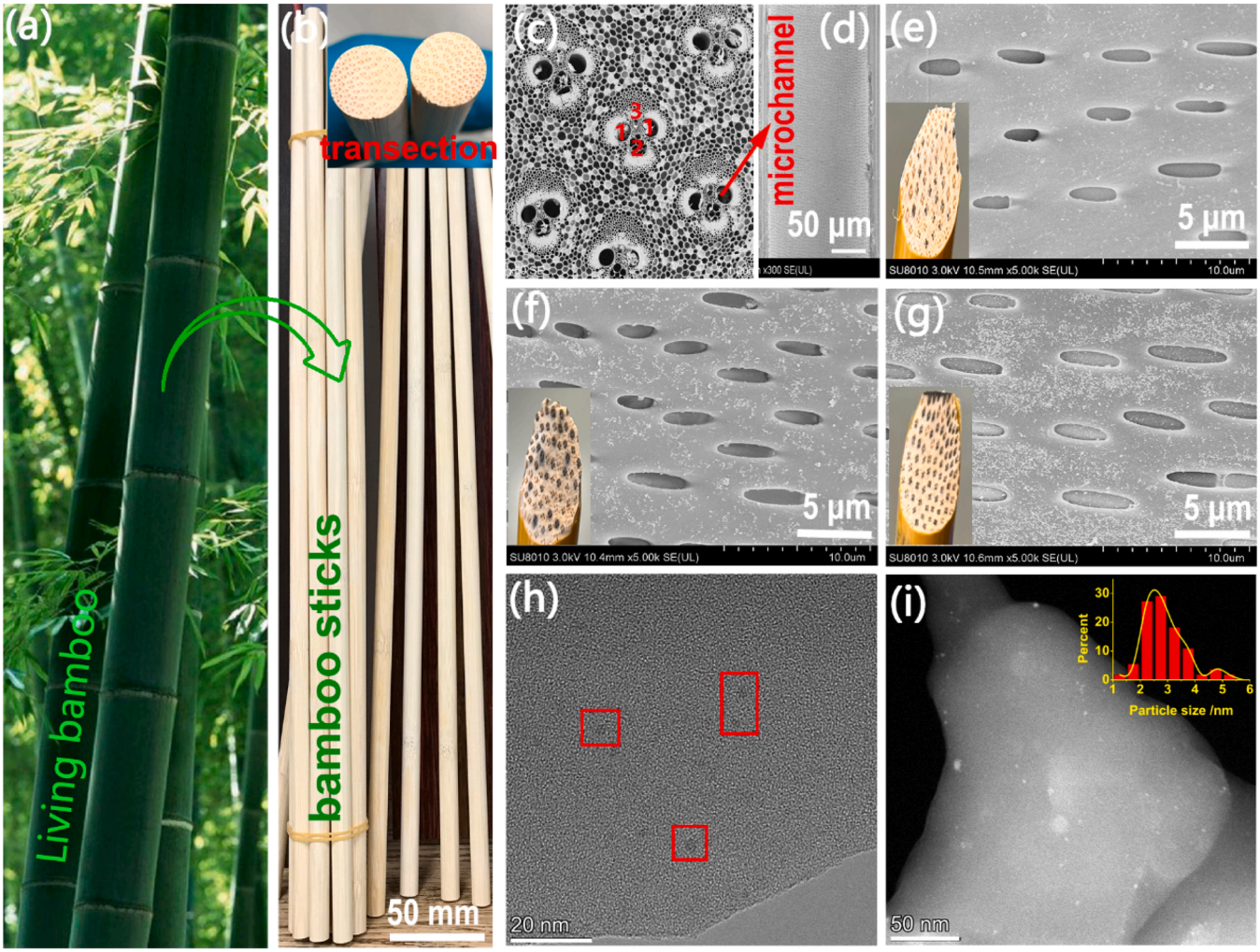


**Fig. 2.** (a) A Moso bamboo sample. (b) The bamboo sticks with uniform column shape and diameter of around 10 mm. The inset in Fig. b is the transection section of a bamboo stick. (c) SEM image of the vascular bundles embedded within a matrix of ground parenchyma cells. The mean diameters of (1) metaxylem, (2) phloem, and (3) protoxylem are 126 μm, 131 μm, and 42 μm, respectively. (d) SEM image of a bamboo microchannel. (e–g) SEM images of bamboo microchannels Ag-1/B CMR (e), Ag-2/B CMR (f), and Ag-3/B CMR (g). The insets are the corresponding oblique section of a sample. (h) TEM image of an Ag-3/B CMR. Ag NPs were observed as indicated by the red box. (i) HAADF-STEM image of an Ag NPs sample. The inset shows the size distribution of the Ag NPs. (For interpretation of the references to colour in this figure, the reader is referred to the web version of this article.)

supported by the color of the oblique section of the bamboo sample (see insets) and EDS mapping results (Fig. S4). Note that the microchannels at either end of a bamboo strip need to be kept completely open, otherwise it was difficult to load the Ag NPs (Fig. S5). In addition, as illustrated in the pore size distribution curve in Fig. S6, the pore diameters of the as-prepared Ag-3/B CMR mainly distribute from nanoscale to microscale, further revealing the hierarchical pore architecture. Its porosity is as high as 57.26%.

The particle size and crystal structure of the fabricated Ag NPs were further determined using TEM (Fig. 2h and S7) and high-angle annular dark-field scanning TEM (Fig. 2i). The Ag NPs showed a spherical shape with no obvious aggregation. The bright spots in the HAADF image corresponded to isolated Ag atoms that remained on the bamboo substrate. The corresponding statistical histogram illustrated that the average size of the formed Ag was 2.9 nm. The small grain size of Ag NPs may have contributed to the high catalytic efficiency of the bamboo-inspired CMR. Meanwhile, the Ag NPs that were synthesized by the static method with the same reaction concentration showed bigger sizes and a wider size distribution (Fig. S8). These results indicated that the flow method was appropriate for the homogenous formation of Ag NPs on the microchannels. The continuous-flow process provided a homogeneous concentration distribution of $Ag(NH_3)_2^+$ ions. It achieved a better contact between the $Ag(NH_3)_2NO_3$ solution and large surface of the microchannel, which contained sufficient reaction sites. We also note that the reaction solutions remained basically colorless during the reactions, suggesting that the immobilized Ag NPs were not released into the solution.

The surface electronic and chemical properties of Ag/B CMR samples were probed by XPS. The main peaks found in all samples at 284.7, 399.8, and 532.6 eV were assigned to C 1 s, N 1 s, and O 1 s, respectively (Fig. 3a). The peaks found in the 373.8–367.8 eV range were observed in the Ag/B CMR samples. These were attributed to the Ag 3d of the Ag NPs. The high-resolution XPS spectrum (Fig. 3b) showed two peaks that were associated with a 3d doublet at 373.8 eV (Ag $3d_{3/2}$) and 367.8 eV (Ag $3d_{5/2}$) with a peak-to-peak distance of 6.0 eV. These were characteristics of metallic Ag, indicating the formation of metallic Ag NPs in the sample [32]. This result was further supported by the XRD analysis, where the Ag-3/B CMR exhibited two sets of diffraction peaks that were not found in untreated bamboo (Fig. 3c). The Ag-3/B CMR showed four new diffraction peaks at $2\theta$ of 38.1°, 44.3°, 64.4°, and 77.4°, which corresponded to the (111), (200), (220), and (311) of a crystal face-centered-cubic crystalline Ag (JCPDS card no. 04–0783) [33].

To further examine the distribution of Ag NPs in a bamboo microstructure, an area of a bamboo substrate including parenchyma cells and

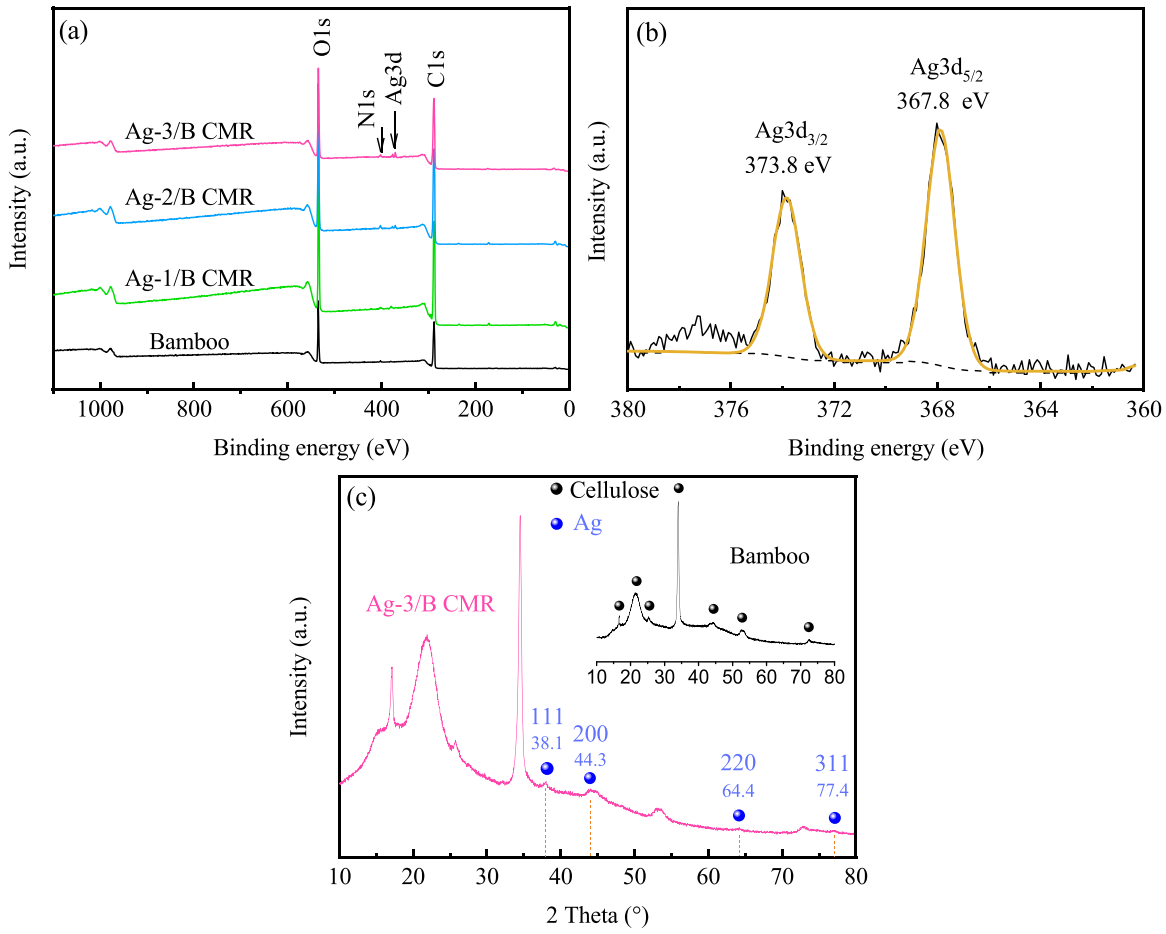


**Fig. 3.** (a) Representative XPS spectra of an original bamboo and Ag/B CMR samples. (b) A representative high-resolution Ag 3d spectrum of Ag-3/B CMR. (c) A representative XRD spectrum of Ag-3/B CMR. The inset is the XRD spectrum of an untreated bamboo.

vascular bundles was mapped by TOF-SIMS (Fig. S9). Visually, there were darker areas in the positive (Fig. 4a) than in the corresponding negative total ion images (Fig. 4d). This observation was attributed to the high cellulose, hemicellulose, and lignin content of bamboo. The positive ion was much lower than negative ion counts of the bamboo substrate. Fig. 4b illustrates the distribution of Ag NPs in the vascular bundles and parenchyma cells. The $Ag^+$ was mainly present in the vascular bundles, and this matched our experimental design. Although the bamboo vascular channel was washed thoroughly, $K^+$ ions were still abundant (Fig. S10) [34]. We note that $C^-$ was evenly present (Fig. 4e), although $CN^-$ was mainly concentrated in the vascular channel of the bamboo sample. This result indicated the efficient reduction of Ag $(NH_3)_2^+$ ions in the vascular channel. We have previously shown that ammonia easily penetrated the bamboo structure, and this caused the breakdown of the oxygen linkages that held the cellulose and hemicellulose polymer chains together [10]. We assumed that lignin could potentially play a crucial role in reducing the $Ag(NH_3)_2^+$ ions to Ag NPs. Therefore, Ag NPs mainly exists in the microchannels of vascular system along with the flow routes.

### 3.2. Mechanical property of the bamboo-inspired CMR

For the practical applications, the flow microreactor must be able to function under appropriate conditions of pressure for a long time. Therefore, the mechanical properties especially the compressive strength were considered. Here, we tested the compressive strength of the Ag-3/B CMR according to the standard method GB/T 1041–92. The load was applied along the longitudinal axis of bamboo sticks. Five samples were tested for each series and the mean values were reported with their standard deviations. Fig. 5a shows the compression strength of the prepared catalytic microreactors. The compression strength of Ag-3/B CMR (47.62 MPa) was slightly better than the untreated bamboo (44.58 MPa). This could be due to the introduction of Ag NPs that were dispersed in the bamboo matrix, concentrated around the microchannels. Our approach also surpassed the performance of various popular cellulose-based [35], metal-based composite [36], graphene/carbon-based [37–40], polymer-based [41], and strong ceramics catalysts [42,43] (Fig. 5b). The bamboo material achieved an unusually high mechanical efficiency (mechanical performance per unit weight) due to their fiber-reinforced cellular structure, where the fibers were aligned parallel to its stem [6]. Notably, compared with catalyst monoliths with high cost or complicated procedures, our approach used a raw material that was derived from a low-cost bamboo (≈0.078 USD/Kg) and simpler preparation process.

### 3.3. Catalyst activity evaluation using model reactions

#### 3.3.1. Effect of different ag loading amounts

In a living bamboo, the bamboo microchannels help pump water upwards through a transpiration process. In our bamboo-inspired design, a peristaltic pump was employed to allow the reactants solution to continuously flow through the microreactor (Fig. 6a, Fig. S11). In our microreactor, the Ag NPs played the role of a heterogeneous catalyst. The catalytic reaction occurred as the reactants flowed through the microreactor. The reduction of 4-NP to 4-aminophenol (4-AP) in the presence of $NaBH_4$ was utilized as a model reaction to evaluate the catalytic performance. This reaction was chosen because this it was easy to operate and can be directly observed from solution color changes. The

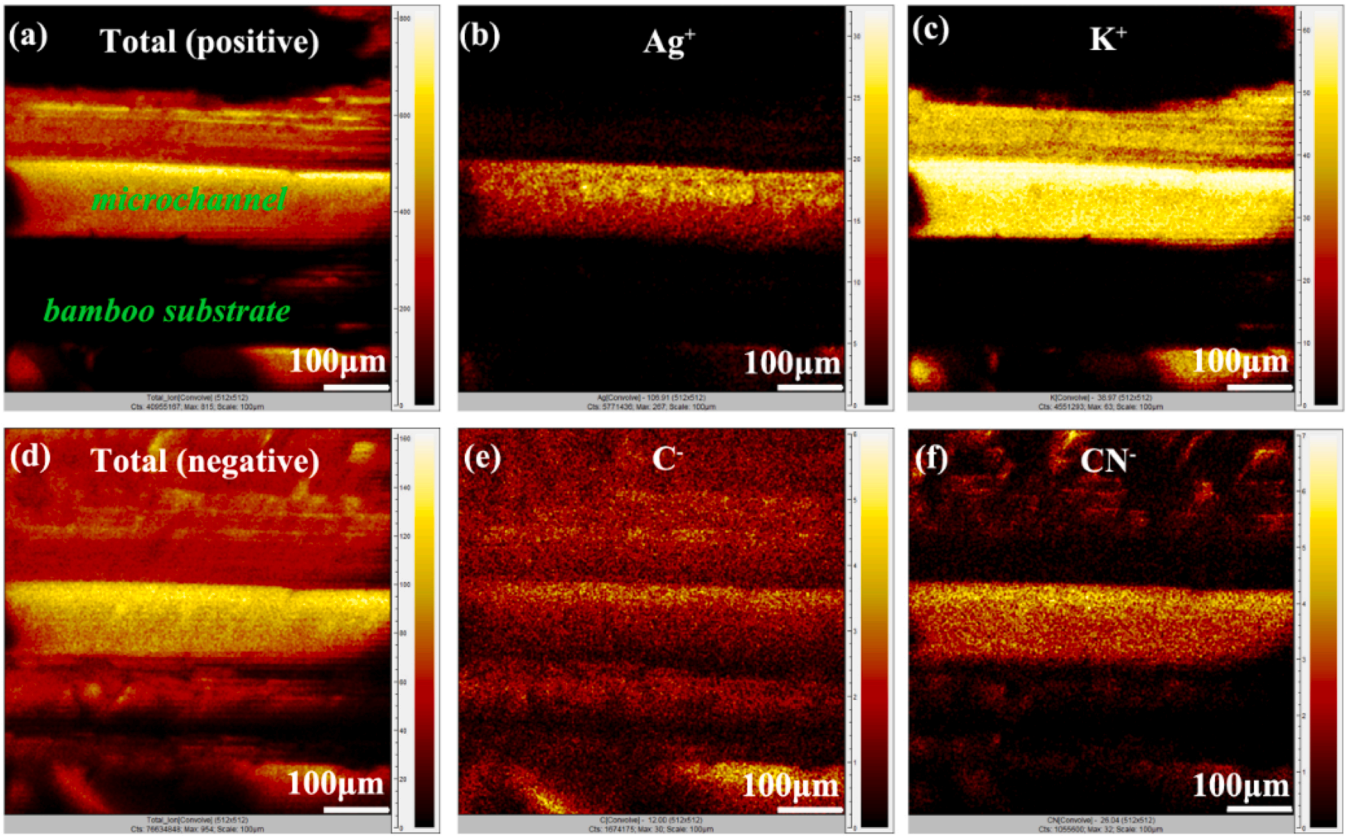


**Fig. 4.** Representative TOF-SIMS ion images of Ag-3/B CMR. (a) Total (positive), (b) $Ag^+$, (c) $K^+$, (d) total (negative), (e) $C^-$, and (f) $CN^-$.

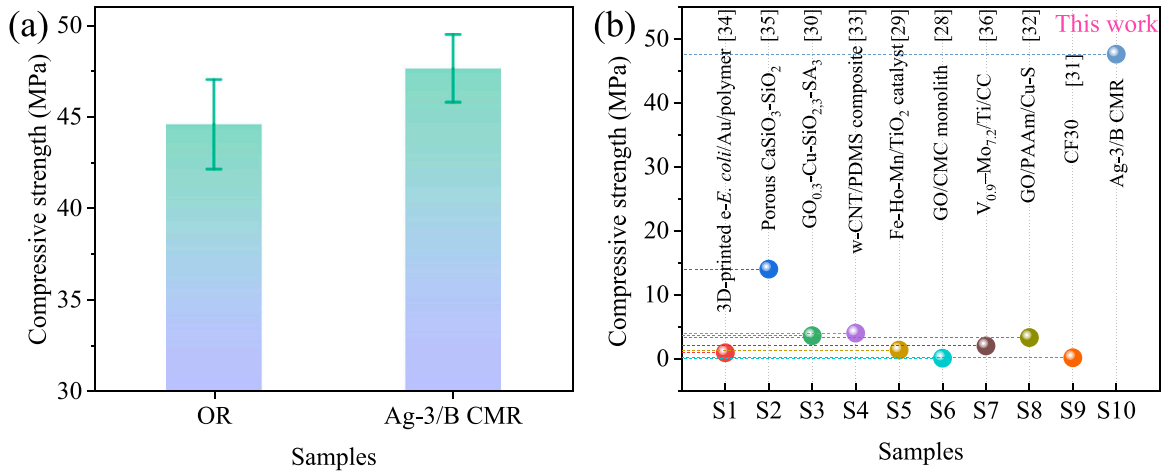


**Fig. 5.** Compressive strength of (a) the original bamboo (OR) and the prepared bamboo-inspired CMR and (b) the popular catalyst using ceramics, metal-based composite, cellulose-based materials, graphene/carbon-based composites, and polymers as support.

color of the reaction solution will change from yellow to colorless [44]. Moreover, the continuous-flow removed the use of sophisticated post treatment or tedious recycle process of catalysts.

In this experiment, a freshly prepared solution containing of 0.5 mM 4-NP and 0.25 M $NaBH_4$ was flowed at 240 μL/min through the microreactor. For comparison, an original bamboo microreactor without Ag catalyst was also investigated in parallel. The absorption maxima (400 nm) of 4-NP did not change and no absorption maxima for product 4-AP at 299 nm was observed as shown in Fig. 6b. These indicated that the bamboo microchannels served as catalyst support only. For the reaction under study, 4-NP reacts with $NaBH_4$ to produce the intermediate 4-nitrophenolate, which converts into 4-AP in with the aid of Ag catalysts [45]. The Ag-1/B CMR (0.15 wt% of Ag) and Ag-2/B CMR 0.36 wt % of Ag) were not able to efficiently convert 4-NP to 4-NA, as shown in Fig. 6b. However, with the Ag-3/B CMR with a higher 0.56 wt% of Ag, only the absorption maxima of 4-AP at 299 nm was clearly observed. The calculated fractional conversion of 4-NP was as high as 97.4%. In summary, the proposed microreactor showed high catalytic activity in the reduction reaction when a sufficient amount of catalyst was embedded in the microchannels.

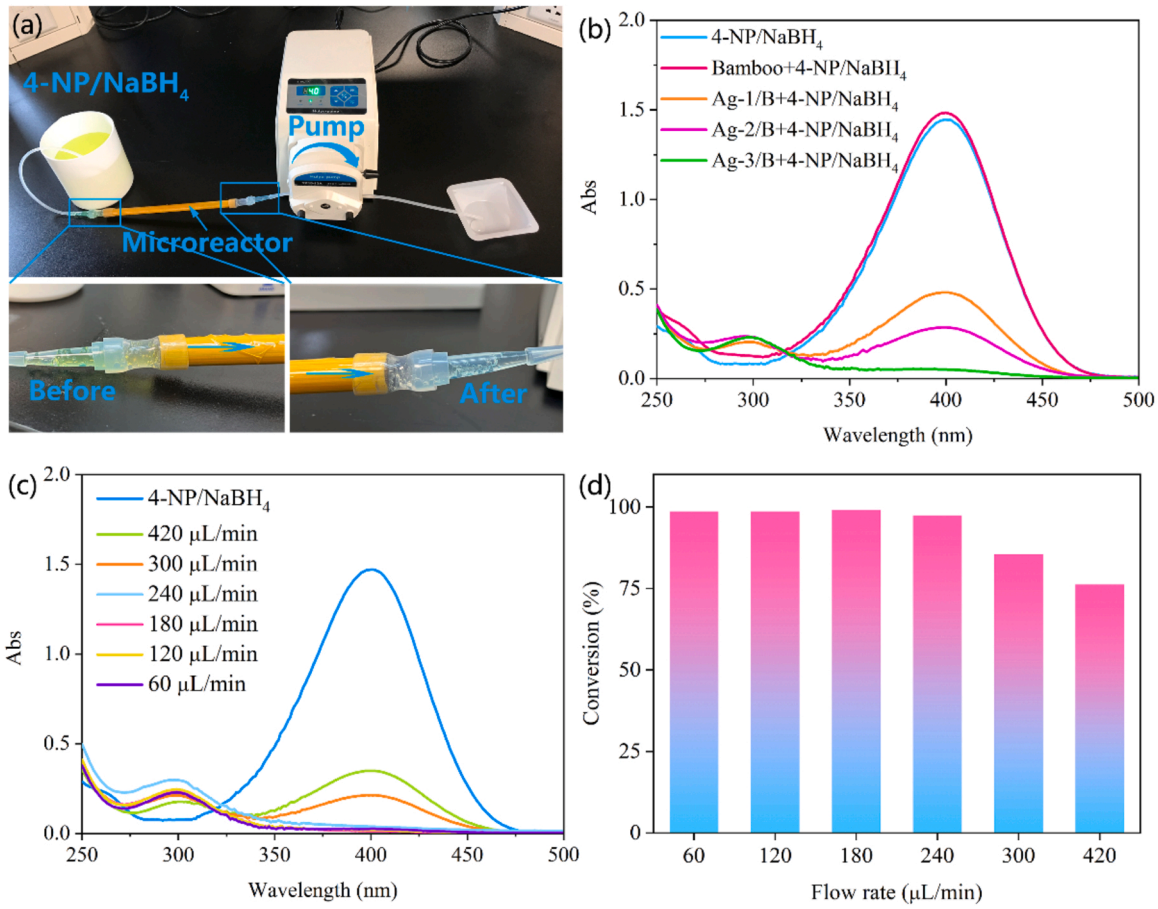


**Fig. 6.** (a) A digital photograph of the flow Ag/B CMR during a catalytic process. (b) UV-Vis spectra of a 4-NP/$NaBH_4$ solution before and after passing through an original microreactor and Ag/B CMR with different Ag loadings at the flow rate of 240 μL/min. (c) UV-Vis spectra of a 4-NP/$NaBH_4$ solution after passing through a Ag-3/B CMR at various flow rates. (d) The conversion efficiency of 4-NP after passing through the Ag-3/B CMR at various flow rates. The reactant solutions were diluted by 3 times before each test.

### 3.3.2. *Effect of the flow rate*

To illustrate the dependency between catalytic conversion and flow rate, the Ag-3/B CMR was used in the reduction of 4-NP. At flow speed of lower than 240 μL/min (Fig. 6c), the peak maxima of 4-NP at 400 nm disappeared and the conversion efficiencies were up to 99% (Fig. 6d). Meanwhile, the efficiencies were lower at flow rates higher than 240 μL/min, and the absorbance maxima of 4-NP at 400 nm was observed. The conversion efficiency declined from 97.4% to 76.2% when the flow was increased from 240 to 420 μL/min, respectively. It was not surprising that the efficiency was highest at the lowest flow rate, since the flow rate is indirectly proportional to the residence time.

### 3.3.3. *Catalytic activity on various nitroaromatics*

To study the scope and generality of the prepared Ag-3/B CMR, the catalytic conversion of other nitroaromatics with different substituents (2-NP, 2-NA, and 4-NA) were also conducted at the flow rate of 120 μL/min, which corresponded to the residence time of 0.79 min 2-NP was easily converted at a flow speed of 120 μL/min as shown in Fig. 7a. The characteristic maxima of 2-NP at around 415 nm disappeared after the reaction. The color of the reactant solution varied from yellow to colorless during the reaction process. Similarly, the 2-NA and 4-NA were also easily degraded within a short time Fig. 7c–f. The intensities decreased at their characteristic maxima of 412 nm (2-NA) and 380 nm (4-NA), respectively. The color of both reactant mixture varied from their natural color to colorless, indicating the conversion finished completely. From previous studies, the 4-NP and 4-NA showed higher reactivity than 2-NP and 2-NA, which was due to the negatively charged O atoms on 4-NP or 4-NA. The ions in 4-NP and 4-NA are delocalized throughout the benzene ring and thus are more resonance-stabilized than those in the 2-NP and 2-NA [44,46]. Hence, 4-NP and 4-NA was used as the model compound for the further experiments.

### 3.3.4. *The stability of bamboo-inspired CMR*

To clarify the storage stability of the microreactor, the prepared Ag-3/B CMR that was stored in our laboratory for 75 days was employed to evaluate catalytic performance. The conversion percent was 98.7% (Fig. S12), which was acceptable. This result suggested that the microchannels were stable in air. The leaching of Ag catalyst was tested by circulating purified water (10 mL) through the Ag-3/B CMR at a flow rate of 120 μL/min for 12 h. The sample water was collected and added into the mixed reactants solution containing 0.5 mM 4-NP and 0.25 M $NaBH_4$. The yellow color of 4-NP did not fade after 5 days Fig. S13a and b, indicating that the leaching of Ag catalyst during the flow process was negligible.

Long-term stability and reusability are essential requirements for the industrial application of the CMR. We evaluated the long-term stability of the microreactor by testing the catalytic ability of Ag-3/B CMR at the flow rate and inlet 4-NA concentration of 120 μL/min and 0.5 mM, respectively. The reusability was performed five consecutive times, each with the same Ag-3/B CMR and a fresh dye solution. At the first cycle, even after continuously using for 14 h, the catalytic efficiency was very high (93.74%), indicating the stability for long time operation (Fig. 8). We carried out the catalytic tests for up to 20 h till the catalytic activity deteriorated. The partial deactivation of Ag-3/B CMR was probably

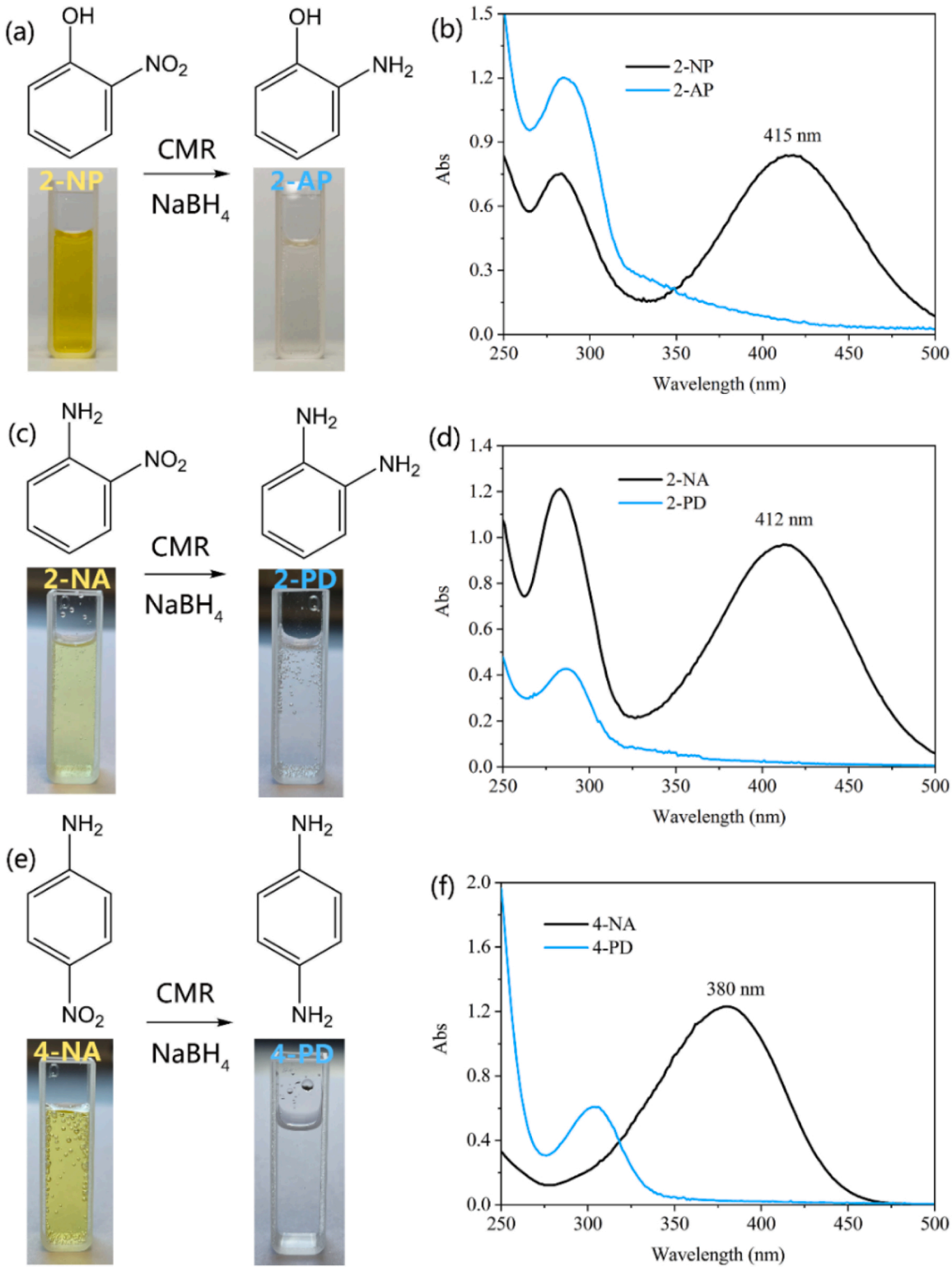


**Fig. 7.** The catalytic conversion of (a, b) 2-NP, (c, d) 2-NA, and (e, f) 4-NA in the Ag-3/B CMR.

caused by the adsorption of the product molecules during the reaction rather than the leaching of Ag NPs. This was because the catalytic performance of Ag-3/B CMR was perfectly recovered after a simple wash-dry process as observed in the latter cycles. After the completion of each catalytic reduction, the Ag-3/B CMR was washed with 50-mL purified water at a flow rate of 120 μL/min and then dried at 45 °C in air for the next catalysis cycle. The Ag-3/B CMR can be reused more than five times for 11 h each time with a stable conversion of above 90% as shown in Fig. 8. This result demonstrated that the bamboo-inspired CMR featured excellent stability and high efficiency for a catalysis reaction in a continuous-flow reaction system.

### 3.3.5. *Practical application for environmental water*

The catalytic activity of bamboo-inspired CMR on environmental

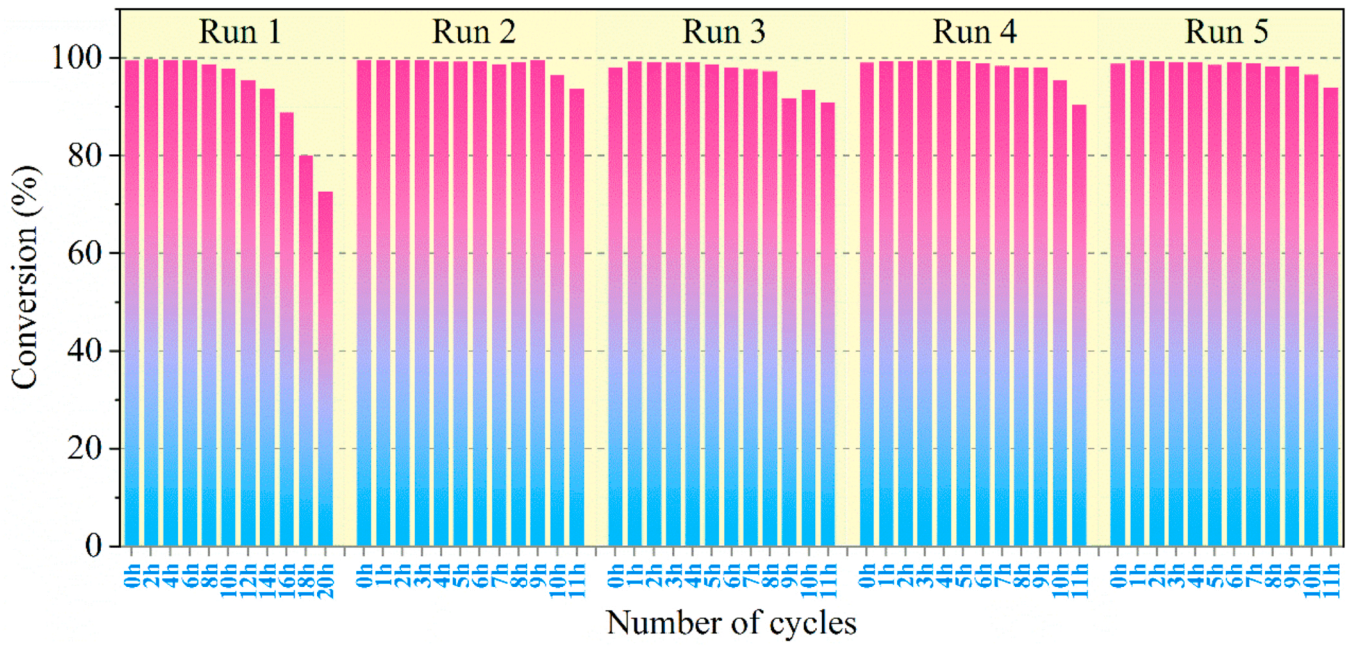


**Fig. 8.** Long-term stability and reusability of the bamboo-inspired CMR.

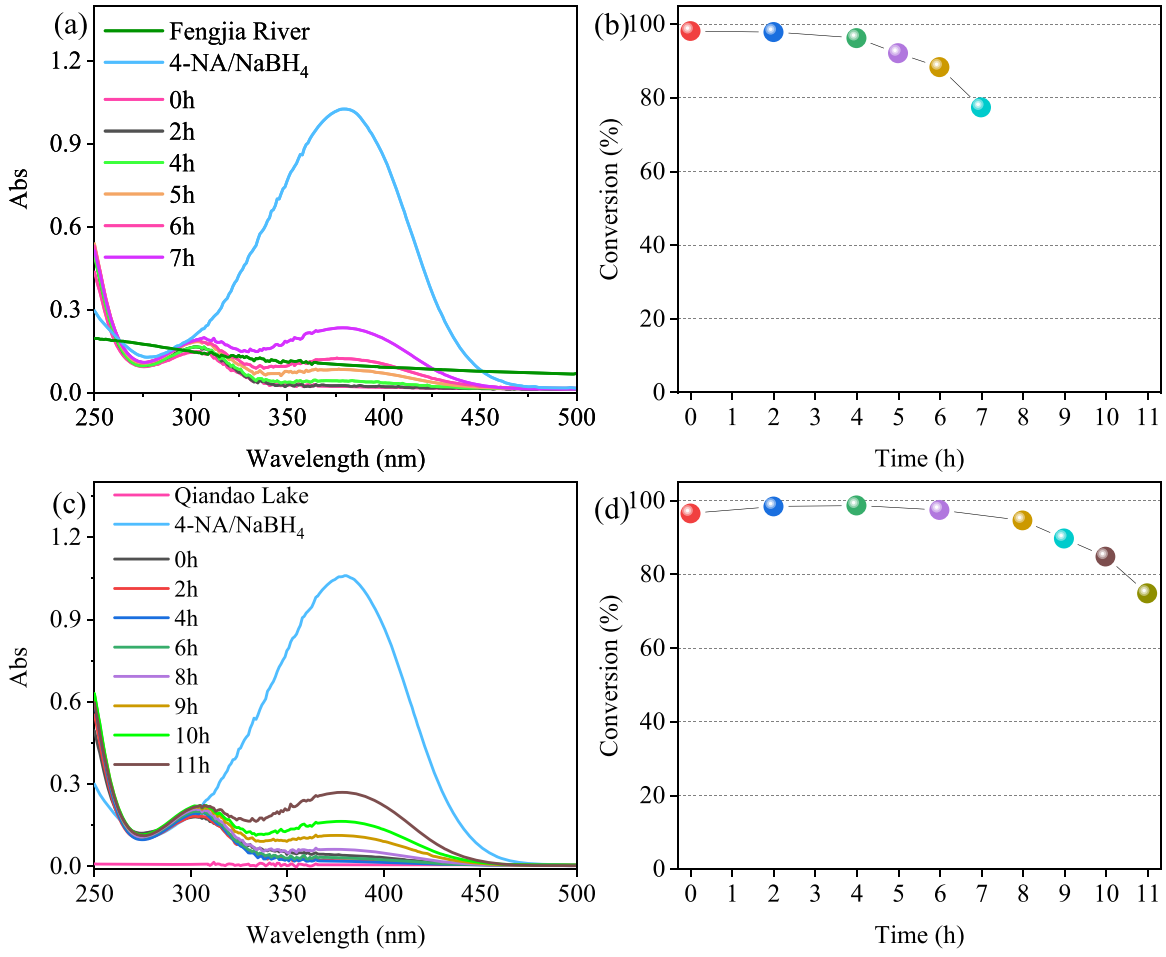


**Fig. 9.** UV–vis spectra and corresponding conversion efficiency of the 4-NA/$NaBH_4$ solution after treatment with the Ag-3/B CMR using (a, b) Fengjia River and (c, d) Qiandao Lake as sample matrix.

water was proposed in this work. We used river water and lake water instead of purified water for the catalytic experiments. The Fengjia River is very turbid and it was impossible to see the bottom of the river even at the shallow areas Fig. S14a. The UV-Vis spectrum of the Fengjia river water sample Fig. 9a indicated the absence of 4-NA. After mixing the sample with 4-NA/$NaBH_4$, the absorption maxima of 4-NA in river water occurred at 380 nm, which suggested the stability of 4-NA in the turbid river water sample. A new absorption maxima was observed at 304 nm after flowing the sample through the Ag-3/B CMR, which revealed the product of 4-PD [27]. The catalytic efficiency was up to 98.15%. The catalytic efficiency remained very high (>88.29%) even after 6 h of continuous loading Fig. 9b. However, the efficiency dropped after 6 h. It has been reported that dissolved oxygen, ions, solution pH, silt, and natural organic matter could affect the reaction process. The partial deactivation of Ag-3/B CMR by river water was probably caused by the adsorption of silt and organic matter Fig. S14a(inset) and b, sediments are presented in the container bottom). Meanwhile, the catalytic efficiency of Ag-3/B CMR with clear Qiandao lake water provided a stable conversion of above 85% for 10 h (Fig. 9c and d). In summary, the Ag-3/B CMR, with high efficiency and stability, can be used as a promising catalyst in practical application.

### 3.4. *Mechanistic insight on the reduction of nitroaromatics by the bamboo-inspired catalytic system*

Considering that the reaction solution that was used to prepare the catalytic system was only $[Ag(NH_3)_2]NO_3$ and water, we proposed that the $Ag^+$ ions was reduced to Ag NPs by the bamboo itself. When the Ag $(NH_3)_2^+$ ions flowed through the bamboo microchannels, the negatively charged bamboo (Fig. S15) that is composed of cellulose, hemicellulose and lignin with abundant oxygen-containing functional groups adsorbed (electrostatic interaction) and reduced the $[Ag(NH_3)_2]^+$ in situ [47–49]. These synthesized and stabilized the monodisperse Ag NPs on the walls of microchannels. Aggregation of Ag NPs at the surface was prevented, providing a large free surface and more reactive sites for catalysis [31].

The mechanism for the hydrogenation of nitroaromatics by the bamboo-inspired CMR system was proposed on the basis of the Langmuir–Hinshelwood mechanism. Using the reduction of 4-NP as example, the continuous-flow reduction process by Ag-3/B CMR included four steps (Fig. 10a) [45]: 1) 4-NP is adsorbed to the Ag catalyst surface; 2) $H^\bullet$ radical species are produced by reaction of $NaBH_4$ with $H_2O$, which are transferred to the Ag surface to form an Ag hydride complex (i.e., Ag–H); 3) the hydrogen transfers from Ag–H to 4-NP; and (4) diffusion of the product 4-AP away from the Ag catalyst surface. Because of the much weaker absorbability of amino groups than that of nitro groups, as-obtained 4-AP once generated would desorb readily from Ag catalyst surfaces, then the reaction can be proceed spontaneously [45].

To further understand the reaction mechanism, EPR measurement with 5,5-dimethylpyrroline N-oxide (DMPO) as spin trapper was proposed to demonstrate the presence of $H^\bullet$ radical species and Ag–H bonds. No obvious EPR signals were detected in the absence of $NaBH_4$, but the signal that consisted of a 1:1:1 triplet of 1:2:1 triplet was detected in the presence of $NaBH_4$ as shown in Fig. 10b. This was identified as a DMPO–H adduct by comparison with a previous study [50]. The $BH_4^-$ generated the $H^\bullet$ radical adducts via dissociation of the B–H bond [44]. Nonetheless, the intensity of the DMPO–H signal was enhanced in the presence of Ag-3/B CMR@$NaBH_4$, illustrating that the DMPO–H adducts were most likely from the abstraction of hydrogen from the active sites of the Ag NPs. However, the intensity of the DMPO–H signal was reduced in the presence of the original bamboo@$NaBH_4$. Thus, the presence of Ag NPs assisted the dissociation of B–H bonds and promoted the abstraction of hydrogen from $NaBH_4$ to form Au-H intermediates [51]. Since the reduction takes place on the active sites of Ag NPs, the catalytic process was considered as a cycle of $H^\bullet$ radical adducts trap and transport steps.

In our bamboo-inspired CMR system, the bamboo monolith showed no catalytic activity but they promoted the catalytic behavior of Ag NPs by anchoring the Ag NPs on their microchannel walls. This avoided the aggregation and leaching of Ag NPs. The monolithic bamboo is different from wood or other biomass materials. It has a special hierarchically porous channel structure that is present all the way through its entire length (e.g., 200 mm). The long, narrow, and accessible channels of the bamboo reactor provided a good permeability, which allowed an effective solution flow with small-resistance. The regular perforated plates that were perpendicular to the flow direction and secondary micropores (pits) on the microchannel wall allowed the additional mixing of the reactants Fig. 10a [29,52,53]. This enabled the reactants to quickly diffuse into the vary narrow channel space and come in contact with the catalysts.

Furthermore, the immobilization of Ag NPs was realized by the flow method. The Ag NPs were mainly formed on the channel surface of the bamboo along with the flow routes with good dispersion. This allowed the optimal use of the Ag in the reaction during the flow process. Therefore, the bamboo-inspired catalytic microreactor provided a combination of good flow ability and high reaction efficiency.

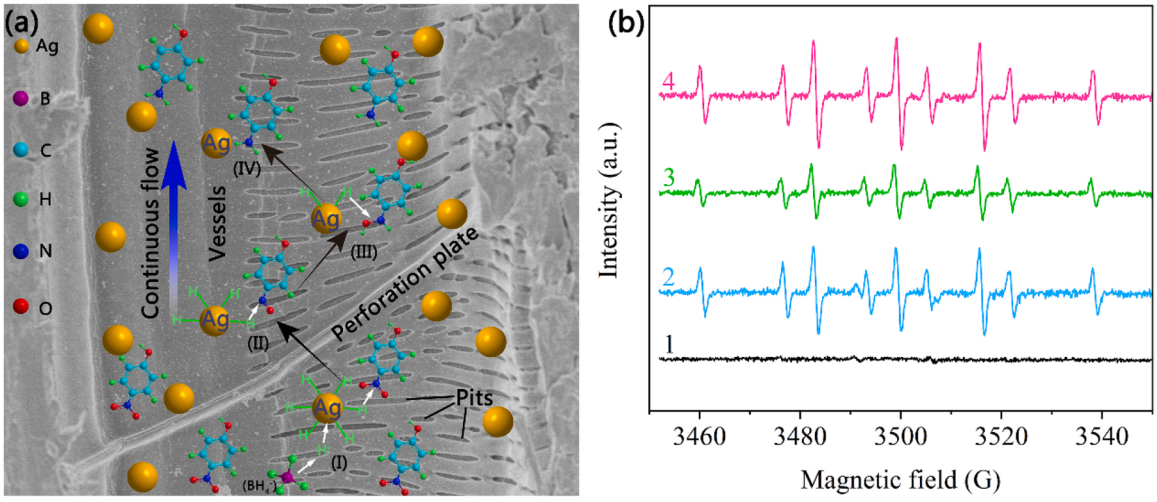


**Fig. 10.** (a) The proposed mechanism for 4-NP reduction in the presence of $NaBH_4$ by Ag-3/B CMR. (b) Representative EPR spectra of DMPO–H adducts, which were formed in the presence of (1) 4-NP@ Ag-3/B CMR, (2) 4-NP@$NaBH_4$, (3) 4-NP@$NaBH_4$ @bamboo, and (4) 4-NP@$NaBH_4$ @ Ag-3/B CMR.

## 4. Conclusions

In this work, we demonstrated a bamboo-inspired design for a stable and high-efficiency CMR, which was used for the reduction of nitro-aromatics. The bamboo-inspired CMR was prepared in room temperature by a simple continuous-flow method, which mimicked the transpiration of bamboo. This approach produced Ag NPs that were uniformly deposited on the walls of the long, interconnected bamboo microchannels without adding any external reductant. Compared to batch synthesis, the flow fabrication was more conducive for the preparation of homogenous Ag NPs with relatively smaller sizes. This consequently reduced the dosage of the catalyst. The bioinspired capillary microreactor inherits all the structural characteristics and mechanical strength of natural bamboo. It allowed effective fluid flow while maintaining the high reactivity of the Ag catalyst anchored on the walls. These characteristics achieved the high catalytic activity of bamboo-inspired microreactor in the reduction of various nitro-aromatics (4-NP, 2-NP, 4-NA, and 2-NA). The microreactor showed good long-term stability (e.g., with continuous-flow catalytic performance of 90% within 11 h over five cycles). In addition, the microreactor was applied to environmental water samples, where it showed high catalytic ability. This bamboo-inspired design should be applicable to other catalytic reactions such as those for continuous hydrogen generation, oxygen evolution, and tar steam reforming. It should also find use with other metals (bimetals) as catalysts.

## CRediT authorship contribution statement

**Jingpeng Li:** Conceptualization, Methodology, Formal analysis, Investigation, Data curation, Writing – original draft, Funding acquisition. **Rumin Ma**: Formal analysis, Software. **Yun Lu**: Conceptualization, Methodology, Formal analysis, Investigation, Funding acquisition. **Zaixing Wu**: Formal analysis, Investigation. **Rong Liu**: Formal analysis, Investigation. **Minglei Su**: Formal analysis, Writing – review & editing. **Xiaobei Jin**: Formal analysis, Investigation. **Rong Zhang**: Formal analysis, Investigation. **Yongjie Bao**: Formal analysis, Investigation. **Yuhe Chen**: Formal analysis, Writing – review & editing. **Daochun Qin**: Methodology, Formal analysis, Investigation, Writing – review & editing. **Dongjiang Yang**: Formal analysis, Resources, Writing – review & editing. **Zehui Jiang**: Conceptualization, Methodology, Formal analysis, Resources, Supervision, Funding acquisition.

## Declaration of Competing Interest

The authors declare that there is no conflict of interests regarding the publication of this paper.

## Acknowledgements

This work was financially supported by Project of Forestry Science and Technology of the Zhejiang Province (2021SY13) and the National Natural Science Foundation of China (Grant Nos. 32101604, 32122058). The authors would like to thank Prof. Rong from Zhejiang University for support of the SEM/EDS analysis and Teacher Liu from Shiyanjia Lab (www.shiyanjia.com) for the ESR analysis.

## Appendix A. Supporting information

Supplementary data associated with this article can be found in the online version at doi:10.1016/j.apcatb.2022.121297.

## References

[1] A. Tanimu, S. Jaenicke, K. Alhooshani, Chem. Eng. J. 327 (2017) 792–821.
[2] C.G. Frost, L. Mutton, Green. Chem. 12 (2010) 1687–1703.
[3] J. Kobayashi, Y. Mori, K. Okamoto, R. Akiyama, M. Ueno, T. Kitamori, S. Kobayashi, Science 304 (2004) 1305–1308.
[4] G. Zhao, T. Liu, B. Wu, B. Chen, C. Chu, Adv. Funct. Mater. 31 (2021), 2100971.
[5] J. Yue, Cataly. Today 308 (2018) 3–19.
[6] U.G. Wegst, H. Bai, E. Saiz, A.P. Tomsia, R.O. Ritchie, Nat. Mater. 14 (2015) 23–36.
[7] M. Zhu, Y. Li, G. Chen, F. Jiang, Z. Yang, X. Luo, Y. Wang, S.D. Lacey, J. Dai, C. Wang, Adv. Mater. 29 (2017), 1704107.
[8] F. Chen, A.S. Gong, M. Zhu, G. Chen, S.D. Lacey, F. Jiang, Y. Li, Y. Wang, J. Dai, Y. Yao, ACS Nano 11 (2017) 4275–4282.
[9] W. Che, Z. Xiao, Z. Wang, J. Li, H. Wang, Y. Wang, Y. Xie, ACS Sustain. Chem. Eng. 7 (2019) 5134–5141.
[10] J. Li, R. Ma, Y. Lu, Z. Wu, M. Su, K. Jin, D. Qin, R. Zhang, R. Bai, S. He, Green. Chem. 22 (2020) 6846–6854.
[11] Q. Zhang, M. Li, B. Luo, Y. Luo, H. Jiang, C. Chen, S. Wang, D. Min, J. Hazard. Mater. 402 (2021), 123445.
[12] Q. Zhang, X. Zhang, M. Chi, Y. Han, H. Jiang, C. Chen, S. Wang, D. Min, Ind. Crop. Prod. 164 (2021), 113392.
[13] C.M. Kuan, R.L. York, C.M. Cheng, Sci. Rep. 5 (2015) 1–11.
[14] D.S. de Sa, R. de Andrade Bustamante, C.E. Rodrigues Rocha, V.D. da Silva, E.J. da Rocha Rodrigues, C. Djenne Buarque Muller, K. Ghavami, A. Massi, O. Ginoble Pandoli, ACS Sustain. Chem. Eng. 7 (2019) 3267–3273.
[15] O.G. Pandoli, R.J.G. Neto, N.R. Oliveira, A.C. Fingolo, C.C. Corrêa, K. Ghavami, M. Strauss, M. Santhiago, J. Mater. Chem. A 8 (2020) 4030–4039.
[16] C. Sheng, N. Yang, Y. Yan, X. Shen, C. Jin, Z. Wang, Q. Sun, Appl. Therm. Eng. 167 (2020), 114712.
[17] J. Li, F. Wu, L. Lin, Y. Guo, H. Liu, X. Zhang, Chem. Eng. J. 333 (2018) 146–152.
[18] R. Liu, S. Zhang, K. Semple, C. Lian, M. Chen, J. Luo, F. Yang, C. Dai, B. Fei, Ind. Crop. Prod. 170 (2021), 113787.
[19] Z. Li, C. Chen, R. Mi, W. Gan, J. Dai, M. Jiao, H. Xie, Y. Yao, S. Xiao, L. Hu, Adv. Mater. 32 (2020), 1906308.
[20] L. Gu, W. Wu, W. Ji, M. Zhou, L. Xu, W. Zhu, For. Policy Econ. 106 (2019), 101947.
[21] J.-C. Buffet, N. Wanna, T.A. Arnold, E.K. Gibson, P.P. Wells, Q. Wang, J. Tantirungrotechai, D. O'Hare, Chem. Mater. 27 (2015) 1495–1501.
[22] S. Wolf, J.U. Lohmann, Nature 565 (2019) 433–435.
[23] X. Xia, B. Shi, L. Wang, Y. Liu, Y. Zou, Y. Zhou, Y. Chen, M. Zheng, Y. Zhu, J. Duan, Exploration 1 (2021) 9–20.
[24] O.G. Pandoli, R.S. Martins, K.L.G. De Toni, S. Paciornik, M.H.P. Maurício, R.M. C. Lima, N.B. Padilha, S. Letichevsky, R.R. Avillez, E.J.R. Rodrigues, K. Ghavami, J. Coat. Technol. Res. 16 (2019) 999–1011.
[25] F. Shen, Y. Wang, G. Qian, W. Chen, W. Jiang, L. Luo, S. Yin*, Appl. Catal. B: Environ. 278 (2020), 119327.
[26] T. Farid, M.I. Rafiq, A. Ali, W. Tang, EcoMat 4 (2022), e12154.
[27] T. Ji, L. Chen, L. Mu, R. Yuan, M. Knoblauch, F.S. Bao, J. Zhu, Appl. Catal. B: Environ. 182 (2016) 306–315.
[28] Z.-T. Xie, T.-A. Asoh, H. Uyama, J. Hazard. Mater. 400 (2020), 123303.
[29] Y. Wang, G. Sun, J. Dai, G. Chen, J. Morgenstern, Y. Wang, S. Kang, M. Zhu, S. Das, L. Cui, Adv. Mater. 29 (2017), 1604257.
[30] H. Chen, Y. Zou, J. Li, K. Zhang, Y. Xia, B. Hui, D. Yang, Appl. Catal. B: Environ. 293 (2021), 120215.
[31] Z.-T. Xie, T.-A. Asoh, Y. Uetake, H. Sakurai, H. Uyama, Carbohyd. Polym. 247 (2020), 116723.
[32] J. Song, C. Yuan, T. Jiao, R. Xing, M. Yang, D.J. Adams, X. Yan, Small 16 (2020), 1907309.
[33] F. Wang, X. Liu, G. Duan, H. Yang, J.Y. Cheong, J. Lee, J. Ahn, Q. Zhang, S. He, J. Han, Small 17 (2021), 2102532.
[34] R. Kumar, N. Chandrashekar, J. For. Res. 25 (2014) 471–476.
[35] Y. Zhang, Y. Liu, X. Wang, Z. Sun, J. Ma, T. Wu, F. Xing, J. Gao, Carbohyd. Polym. 101 (2014) 392–400.
[36] T. Huang, Y. Zhang, K. Zhuang, Y. Zhu, S. Kai, J. Fuel Chem. Technol. 46 (2018) 319–327.
[37] Y. Hou, X. Zhong, Y. Ding, S. Zhang, F. Shi, J. Hu, Carbohyd. Polym. 245 (2020), 116490.
[38] Y. Zhang, M. Zhao, H. Wang, H. Hu, R. Liu, Z. Huang, C. Chen, D. Chen, Z. Feng, Bioresour. Technol. 288 (2019), 121532.
[39] C. Shan, L. Wang, Z. Li, X. Zhong, Y. Hou, L. Zhang, F. Shi, Carbohyd. Polym. 203 (2019) 19–25.
[40] F. Zhang, Y. Feng, M. Qin, T. Ji, F. Lv, Z. Li, L. Gao, P. Long, F. Zhao, W. Feng, Carbon 145 (2019) 378–388.
[41] L. Long, R. Pei, Y. Liu, X. Rao, Y. Wang, S.-f Zhou, G. Zhan, J. Hazard. Mater. 423 (2022), 126983.
[42] M. Casas-Luna, J.A. Torres-Rodríguez, O.U. Valdés-Martínez, N. Obradović, K. Slámečka, K. Maca, J. Kaiser, E.B. Montúfar, L. Čelko, Ceram. Int. 46 (2020) 8853–8861.
[43] Y. Qiu, B. Liu, J. Du, Q. Tang, Z. Liu, R. Liu, C. Tao, Chem. Eng. J. 294 (2016) 264–272.
[44] Y. Fu, L. Qin, D. Huang, G. Zeng, C. Lai, B. Li, J. He, H. Yi, M. Zhang, M. Cheng, X. Wen, Appl. Catal. B: Environ. 255 (2019), 117740.
[45] S. Jiang, L. Wang, Y. Duan, J. An, Q. Luo, Y. Zhang, Y. Tang, J. Huang, B. Zhang, J. Liu, Appl. Catal. B: Environ. 283 (2021), 119592.
[46] L. Qin, Z. Zeng, G. Zeng, C. Lai, A. Duan, R. Xiao, D. Huang, Y. Fu, H. Yi, B. Li, Appl. Catal. B Environ. 259 (2019), 118035.
[47] Y. Luo, S. Shen, J. Luo, X. Wang, R. Sun, Nanoscale 7 (2015) 690–700.
[48] M. Montazer, F. Alimohammadi, A. Shamei, M.K. Rahimi, Carbohyd. Polym. 87 (2012) 1706–1712.
[49] S. Chen, G. Wang, W. Sui, A.M. Parvez, C. Si, Green. Chem. 22 (2020) 2879–2888.
[50] L. Qin, H. Yi, G. Zeng, C. Lai, D. Huang, P. Xu, Y. Fu, J. He, B. Li, C. Zhang, J. Hazard. Mater. 380 (2019), 120864.

[51] T.B. Nguyen, C. Huang, R.-a Doong, Appl. Catal. B: Environ. 240 (2019) 337–347.
[52] T. Xu, L. Zhang, Z. Li, Sci. Rep. 10 (2020) 1–10.
[53] P.J. Schulte, J. Exp. Bot. 50 (1999) 1179–1187.